EXAFS studies of changes in the local environment of Cu ions in Fe- and Zn-doped $YBa_2Cu_3O_{7-\delta}$ superconductor

1994 J. Phys.: Condens. Matter 6 6865

(http://iopscience.iop.org/0953-8984/6/34/018)

J. Phys.: Condens. Matter 6 (1994) 6865–6874. Printed in the UK

EXAFS studies of changes in the local environment of Cu ions in Fe- and Zn-doped $YBa_2Cu_3O_{7-\delta}$ superconductor

S K Deshpande†, S B Ogale†, S M Chaudhari‡ and A V Pimpale‡

† Department of Physics, University of Poona, Pune 411007, India

‡ Inter-University Consortium for DAE Facilities, University Campus, Khandwa Road, Indore 452001, India

Received 19 April 1994

Abstract. EXAFS spectra have been measured at the Cu K edge in Fe- and Zn-doped $YBa_2Cu_3O_{7-\delta}$ using a laboratory EXAFS spectrometer. The dopant concentration was varied and the changes in the near-neighbour environment around the Cu ions were examined by determining the best-fit structural parameters after curve fitting to the first-shell EXAFS function. The average Cu–O distance is found to decrease as Fe concentration increases, and is found to increase as Zn concentration increases. The results indicate that Fe and Zn affect the Cu–O environment significantly but in different ways. The mobile hole concentration in the $YBa_2Cu_3O_{7-\delta}$ superconductor is known to change with doping, and our results indicate that the Cu–O distance and the mobile hole concentration are probably related, the Cu–O distance increasing as mobile hole concentration decreases and vice versa.

1. Introduction

The $YBa_2Cu_3O_{7-\delta}$ (1:2:3) high-temperature superconductor is the most widely studied of all high-T_c superconductors discovered so far. This material has proved to be very suitable for carrying out studies aimed at understanding the very nature of high-temperature superconductivity. The structure of the 1:2:3 compound is a distorted perovskite. The O-rich $YBa_2Cu_3O_{7-\delta}$ ($\delta < 0.2$) is orthorhombic with lattice constants $a = 3.8231$ Å, $b = 3.8864$ Å and $c = 11.6808$ Å [1]. There are two types of Cu site in the unit cell—the Cu(1) sites forming the Cu–O chains along the b axis and the Cu(2) sites forming CuO_2 sheets in the a–b plane (see figure 1). The effect of substituting the constituent atoms by other elements has been a subject of interest and many substitutional studies have been carried out. It has been shown that substitution at the Cu sites leads to an unfavourable effect on the superconductivity [2–6], indicating that the Cu sites play a decisive role in superconductivity. The site preference of different dopant ions has been exploited in order to determine the relative importance of the two Cu sites. It has been shown [2] that suppression of T_c is more rapid in the case of doping with Ni and Zn, which occupy the Cu(2) sites [7, 8], than in the case of doping with trivalent ions such as Fe, Al or Co, which occupy the Cu(1) sites [2, 3], implying that the Cu(2) sites are more important for superconductivity. It is also observed that the structural symmetry changes from orthorhombic to tetragonal at certain concentrations of Fe, Al and Co, and remains tetragonal for higher concentrations [2].

Since the superconducting properties are closely linked with the structure, it is important to understand the changes in the structure upon substitution with different ions. The technique of extended x-ray absorption fine structure (EXAFS) is very useful for this purpose

0953-8984/94/346865+10$19.50

because of its ability to yield accurate information about the local order around an atomic species in a material. In fact, several EXAFS studies have been carried out on doped 1:2:3 compounds [9–12]. Although the environment of dopant ions has been probed in detail, relatively few studies have been carried out on the Cu environment, especially in the case of Zn doping. Also, the results of studies on changes in Cu environment on Fe doping seem to disagree. For example, Oyanagi *et al* [10] report no change in Cu valence or in the Cu–O environment. Koizumi *et al* [11] report a small change in the Cu(1)–O(4) distance (refer to figure 1). In order to probe this issue further, we have undertaken the present study of the local order around Cu sites in Fe- and Zn-doped 1:2:3. The changes in Cu–O environment as a function of dopant concentration were studied. The differences between the site preferences of these two dopant ions, and between their electronic structures, is expected to affect the local structure differently, and we have attempted to elucidate such effects by using the power of EXAFS for local-structure determination. We describe the experimental details in section 2 and the data analysis procedure in section 3. Our results are discussed in section 4 and we conclude with a brief summary in section 5.

2. Experimental details

The $YBa_2Cu_3O_{7-\delta}$, $YBa_2Cu_{3-x}Fe_xO_{7-\delta}$ ($x = 0.01, 0.1, 0.2, 0.36$), and $YBa_2Cu_{3-x}Zn_xO_{7-\delta}$ ($x = 0.01, 0.1, 0.2, 0.3$) compounds were prepared by the conventional solid-state reaction technique [2]. High-purity Y_2O_3, $BaCO_3$, CuO, ZnO and Fe_2O_3 powders were mixed together in proper proportions. After thorough mixing, the powders were calcined at 950 °C for 48 h with intermittent grinding. The powders were then pressed to 10 mm diameter pellets using a die. The pellets were sintered in air at 950 °C for 24 h. These were then annealed in O_2 at 900 °C for 24 h, and at 600 °C for another 24 h. The pellets were finally furnace cooled to room temperature in flowing O_2.

The compounds were characterized by x-ray diffraction, using a Philips PW1840 powder diffractometer with Cu Kα radiation. All diffraction patterns indicated that the appropriate single phase has been formed. The orthorhombic-to-tetragonal transition for the Fe-doped case was clearly seen for $x = 0.1$, and the structure was found to remain tetragonal for all higher values of x. The Zn-doped compounds remained orthorhombic throughout the range of concentrations studied.

The superconducting transition temperature T_c was measured using a low-temperature four-probe resistivity apparatus. The undoped 1:2:3 compound showed a sharp transition at 92 K and T_c was observed to decrease progressively with doping.

For the EXAFS measurements, the pellets of each sample were finely ground and sieved through a 400 mesh sieve to obtain very small particles of size < 40 μm. The powder was spread uniformly on ordinary adhesive tape and successive layers were added to optimize thickness. The EXAFS spectra were recorded at the Cu K edge using the automated linear EXAFS spectrometer developed in our laboratory [13]. The 12 kW Cu rotating-anode x-ray source was operated at 20 kV and 180 mA, and a Si(311) Johansson crystal of 400 mm Rowland radius was used as monochromator. A single scintillation detector was used to measure x-ray intensity and the sample was oscillated in and out of the beam path. The receiving slit width was 50 μm. Each spectrum was recorded in about 8 h at room temperature. The energy scale was calibrated by using the Cu K$\beta_{1,3}$ emission line, which was assigned energy 8905.14 eV. All spectra were normalized to an edge height of 1.0. Figure 2(*a*) and (*b*) shows the absorption spectra of the Fe- and Zn-doped samples, respectively.

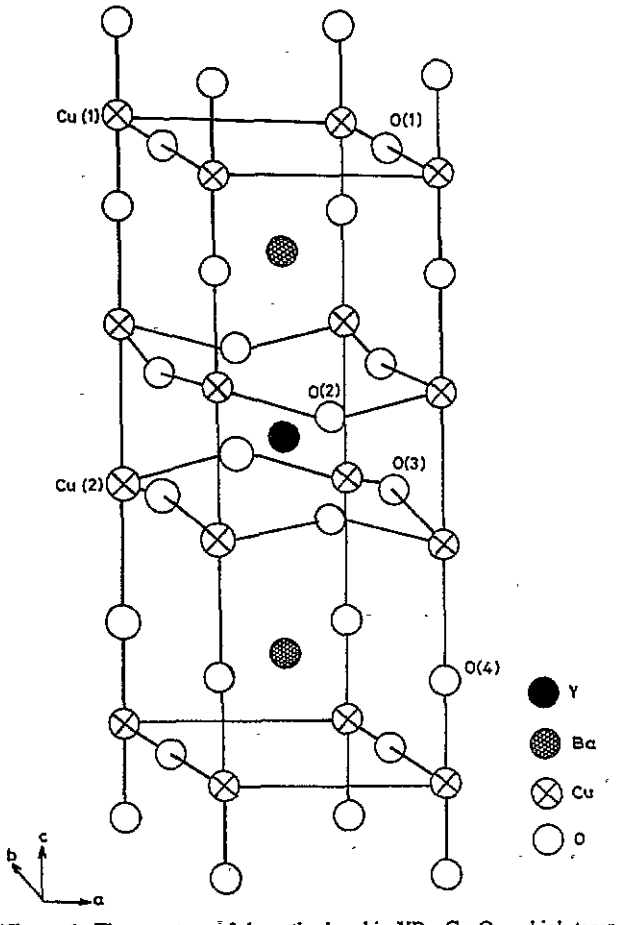

Figure 1. The structure of the orthorhombic $YBa_2Cu_3O_{7-\delta}$ high-temperature superconductor.

3. Data analysis

The data were analysed using a self-contained program package for analysis of EXAFS data [14]. The pre-edge absorption background was removed using a Victoreen function [15]. The μ_0 background fit was carried out using a cubic spline data-smoother routine [16]. The normalized EXAFS function in photoelectron wave-vector space was calculated from the equation

$$\chi(k) = (\mu(k) - \mu_0(k))/\mu_0(k) \tag{1}$$

where $\mu(k)$ is the measured absorption and k is the photoelectron wave vector related to the absorbed photon energy E by

$$E = \hbar^2 k^2/2m + E_0. \tag{2}$$

The value of the threshold energy E_0 was chosen as the mid-point of the total edge height of the Cu K edge in each spectrum. The value of E_0 thus obtained was 8988 eV. No

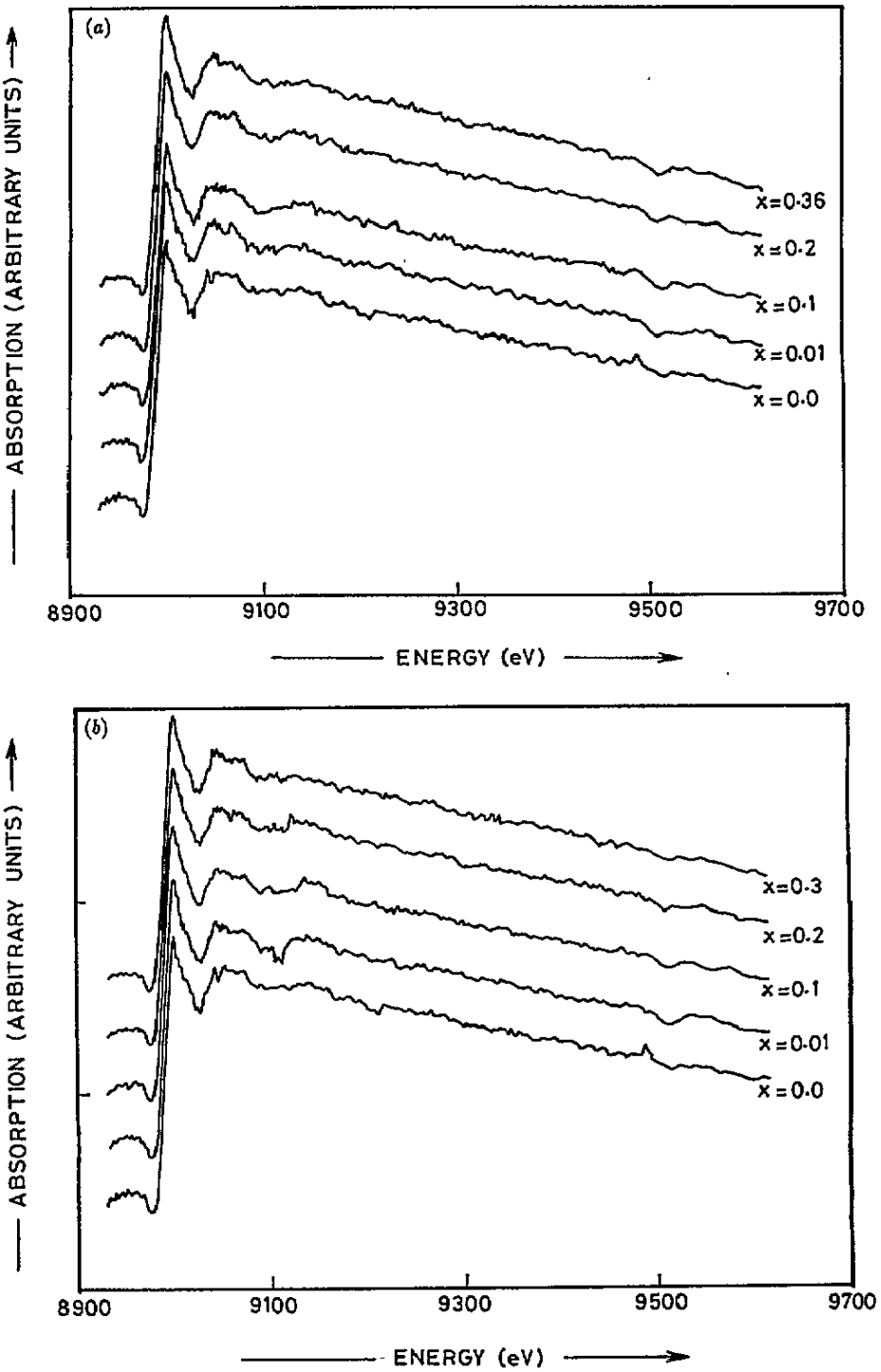

Figure 2. (*a*) The EXAFS spectra of $YBa_2Cu_{3-x}Fe_xO_{7-\delta}$ compounds at the Cu K edge and (*b*) the EXAFS spectra of $YBa_2Cu_{3-x}Zn_xO_{7-\delta}$ compounds at the Cu K edge. All spectra have been normalized to an edge height of unity and shifted vertically for clarity.

change in the edge position was observed as a function of doping, implying that there is no significant change in the effective Cu valence. A fast-Fourier-transform (FFT) routine was used to Fourier transform $k^2\chi(k)$ over a range of 2.4–7.9 $Å^{-1}$. A symmetric Hanning window was used to minimize truncation error. The Fourier-transform magnitude peaks at distances corresponding to the radial distances of near-neighbour coordination shells around the Cu atom.

The first strong peak, which is due to the O nearest neighbours, was Fourier transformed into k space to obtain the first-shell EXAFS $\chi_1(k)$. A rectangular window was used. This first-shell EXAFS function can be expressed as [15]

$$\chi_1(k) = A_1(k)\sin(2kR_1 + \phi_1(k)) \tag{3}$$

with

$$A_1(k) = (N_1/kR_1^2)S_0^2F_1(k)\exp[-2(\sigma_1^2k^2 + (R_1 - \Delta)/\lambda)]. \tag{4}$$

Here, N_1 and R_1 are the number of nearest neighbours (assumed identical) and their average separation from the central atom in the spherical approximation, respectively. $F_1(k)$ is the backscattering amplitude, $S_0^2(k)$ is the amplitude reduction factor due to many-electron effects, σ_1^2 is the root mean squared deviation of the neighbours from R_1, λ is the electron mean-free path, and Δ is the quantity occurring in the inelastic loss term due to many-electron effects. $\phi_1(k)$ is the total phase shift due to the central atom and the backscatterers. R_1 and N_1 can be obtained by curve fitting to $\chi_1(k)$ if $\phi_1(k)$ and the other parameters in $A_1(k)$ are known.

Since the structure of the undoped $YBa_2Cu_3O_{7-\delta}$ is well known and since it is structurally and chemically similar to the doped compounds, we have used it as a structural standard and determined $A_1(k)$ and $\phi_1(k)$ for this phase. The amplitude and phase shifts thus determined were transferred to the doped cases assuming amplitude and phase transferability to be valid [17]. To determine $A_1(k)$ and $\phi_1(k)$, we have used the weighted averages of R_1 and N_1. From figure 1, we see that there are two fivefold-coordinated Cu(2) sites and one fourfold-coordinated Cu(1) site in the orthorhombic unit cell, and the weighted average N_1 is thus 4.67. Using the Cu–O distances determined by neutron diffraction [1], we obtained the weighted-average Cu–O distance as $R_1 = 1.963$ Å. The amplitude and phase shifts have been parameterized as

$$A_1(k) = (N_1/R_1^2)C_0\exp(-C_1k^2)/k^{C_2} \tag{5}$$

and

$$\phi_1(k) = a_0 + a_1k + a_2k^2. \tag{6}$$

These forms are known to approximate the observed EXAFS amplitude and phase shifts very well [18]. The variable parameters C_0, C_1, C_2, a_0, a_1 and a_2 must be determined by fitting these functional forms to the experimentally determined amplitude and phase shifts, and using the above values of N_1 and R_1. Since $\chi_1(k)$ is a sine function it will become zero at values k_n such that

$$2k_nR_1 + \phi_1(k_n) = n\pi \qquad n = 0, 1, 2, 3, \ldots. \tag{7}$$

The values of ϕ_1 at the zeros of $\chi_1(k)$ were determined and (6) was then fitted to these values to obtain the parameters a_0, a_1 and a_2. The parameters C_0, C_1 and C_2 were determined by a multiparameter least-squares fit to the amplitude envelope of $\chi_1(k)$.

Keeping C_0, C_1, C_2, a_0, a_1 and a_2 fixed, the parameters N_1 and R_1 for the doped compounds were determined by allowing them to vary in the least-squares curve-fitting procedure. The best-fit values of N_1 and R_1 will give the average O coordination number and Cu–O distance, respectively. This curve fitting was carried out over a k range of about 2.4–7.8 $Å^{-1}$.

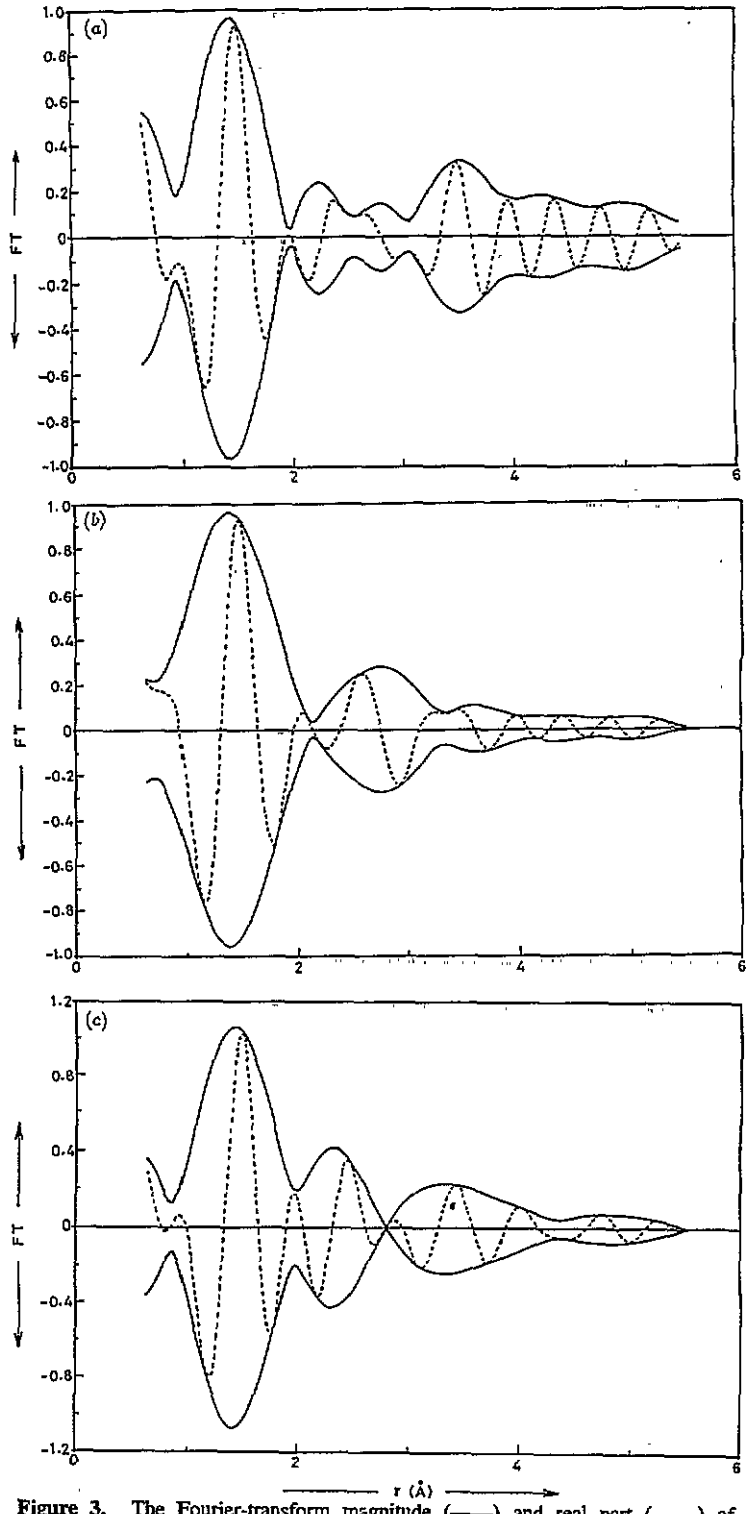

Figure 3. The Fourier-transform magnitude (——) and real part (– – –) of $k^2\chi(k)$ for (*a*) undoped $YBa_2Cu_3O_{7-\delta}$ ($x = 0.0$), (*b*) $YBa_2Cu_{3-x}Fe_xO_{7-\delta}$, $x = 0.1$ and (*c*) $YBa_2Cu_{3-x}Zn_xO_{7-\delta}$, $x = 0.1$.

4. Results and discussion

Figure 3 shows the magnitude and real part of the Fourier transform for undoped 1:2:3, and for the $x = 0.1$ case in the doped compounds. The strong peak at about 1.4 Å is due to O nearest neighbours around Cu. The values of the amplitude and phase-shift parameters of equations (5) and (6), respectively, were obtained for the undoped 1:2:3 compound after inverse transforming this first peak into k space and curve fitting to $\chi_1(k)$. The values are given in table 1 and the curve-fit result is shown graphically in figure 4. The results of curve fitting to $\chi_1(k)$ for the doped compounds are summarized in tables 2 and 3. Figure 5 shows typical fits for $x = 0.1$. The average Cu–O bond distance decreases slightly with increasing Fe concentration, reaching a value of about 1.93 Å for $x = 0.36$. On the other hand, it increases slightly with Zn doping, reaching a value of about 1.99 Å for $x = 0.3$. The behaviour of N_1 is more complicated and does not show a clear trend towards increasing or decreasing. However, it must be borne in mind that the value of N_1 as determined by our procedure includes the effects of changes in the σ_1^2 factor of equation (4) since we have not allowed the shape of the amplitude envelope to vary [18]. In other words, the changes in N_1 reflect a change in O coordination number as well as a possible change in the Debye–Waller factor σ_1^2. Varying C_1 in addition to N_1 and R_1 would allow the shape of the amplitude to vary and give a better fit at the cost of another variable that is correlated with N_1. In our study, however, we have avoided this additional freedom in curve fitting and hence it is not possible to infer much about the behaviour of N_1.

Table 1. The amplitude and phase-shift parameters obtained after curve fitting to the first-shell EXAFS function for the undoped $YBa_2Cu_3O_{7-\delta}$ compound (see the text).

N_1^a	R_1^a	C_0	C_1	C_2	a_0	a_1	a_2
4.67	1.963 Å	0.038 54	0.048 82	−0.207	2.515	−1.28	0.0218

[a] Weighted average of the known values from [1].

Table 2. Structural parameters for Fe-doped $YBa_2Cu_3O_{7-\delta}$ obtained after curve fitting to first-shell data.

x	N_1	R_1 (Å)
0.01	4.55 ± 0.40	1.967 ± 0.020
0.1	5.60 ± 0.40	1.956 ± 0.020
0.2	4.96 ± 0.40	1.965 ± 0.020
0.36	4.90 ± 0.40	1.928 ± 0.020

Table 3. Structural parameters for Zn-doped $YBa_2Cu_3O_{7-\delta}$ obtained after curve fitting to first-shell data.

x	N_1	R_1 (Å)
0.01	5.48 ± 0.40	1.971 ± 0.020
0.1	5.05 ± 0.40	1.974 ± 0.020
0.2	4.55 ± 0.40	1.986 ± 0.020
0.3	5.06 ± 0.40	1.986 ± 0.020

It is interesting that the mobile hole concentration in $YBa_2Cu_3O_{7-\delta}$ has been observed to change with doping [19] and the change in Cu–O bond lengths appears to be related to the mobile hole concentration. The holes on the Cu(1) (chain) sites are known to be localized and only the holes at the Cu(2) (planar) sites are mobile [20]. It has been shown that the mobile hole concentration decreases with increasing Zn in the 1:2:3 compound [19] and our results indicate that the average Cu–O distance increases as the mobile hole concentration decreases. The average number of holes per Cu in the unit cell is dependent on the O content [19]. Therefore, since the O content increases with Fe doping [2], the average number of holes per Cu site in the $YBa_2Cu_3O_{7-\delta}$ unit cell will increase and this in turn will increase the mobile hole concentration. Our results show a decrease in the Cu–O distance as Fe increases, indicating that an increase in the mobile hole concentration is accompanied by a decrease in the Cu–O distance.

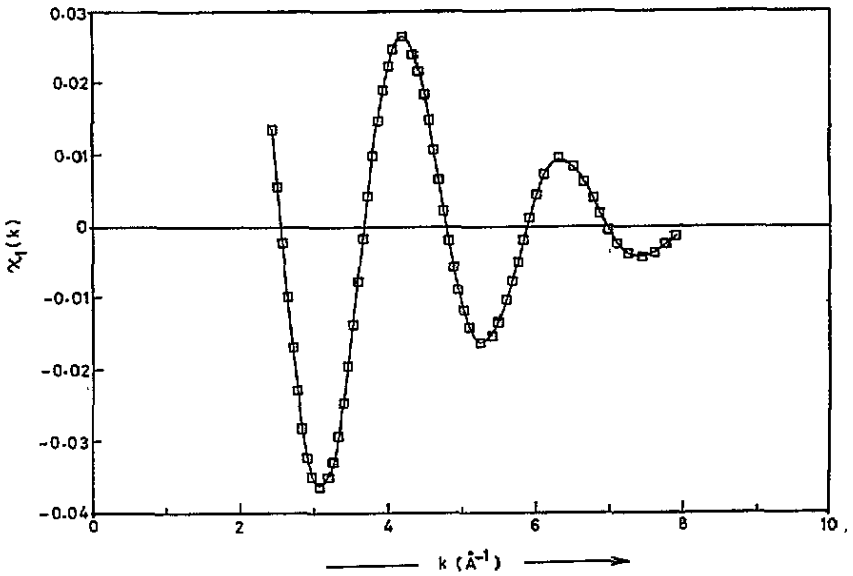

Figure 4. The result of curve fitting to the first-shell EXAFS function for undoped $YBa_2Cu_3O_{7-\delta}$ over a k range of 2.4–7.8 Å^{-1} (□, experiment; ——, calculated curve).

Thus, it appears that the Cu–O distance is related to the mobile hole concentration. The effect of Fe doping on the Cu–O distance is exactly opposite to that of Zn doping and so is the effect on the mobile hole concentration.

5. Summary

Our study on the local environment of Cu in Fe- and Zn-doped $YBa_2Cu_3O_{7-\delta}$ high-T_c superconductor shows that the average Cu–O distance decreases with increasing Fe and increases with increasing Zn. The Cu–O distances appear to be related to the mobile hole concentration, which is crucial for superconductivity in this compound. The Cu–O distance increases with increasing Zn while the mobile hole concentration is known to decrease. For the Fe-doped cases, the Cu–O distance decreases while the mobile hole

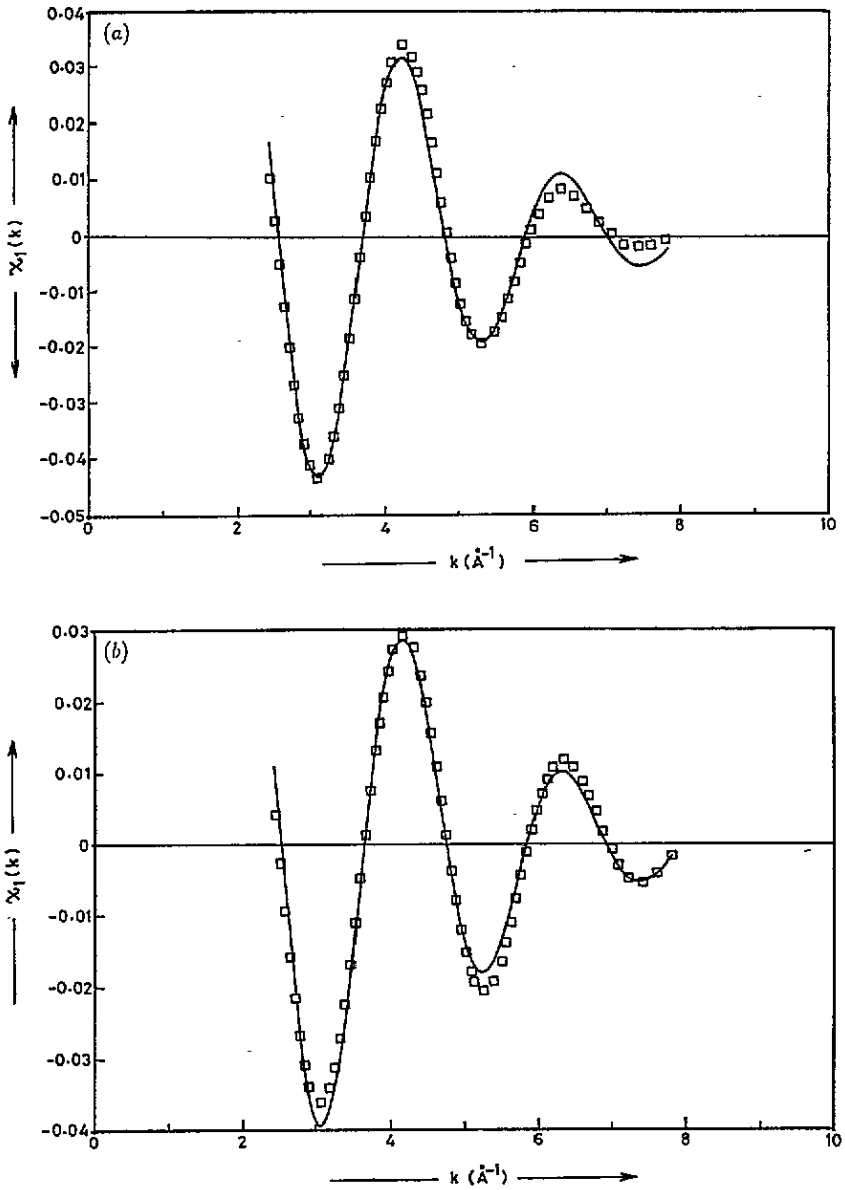

Figure 5. Curve fit results for (*a*) $YBa_2Cu_{3-x}Fe_xO_{7-\delta}$, $x = 0.1$ and (*b*) $YBa_2Cu_{3-x}Zn_xO_{7-\delta}$, $x = 0.1$, over 2.4 Å$^{-1} \leqslant k \leqslant 7.8$ Å^{-1} (□, experiment; ——, calculated curve).

concentration increases with increasing dopant concentration. The Cu–O distance thus seems to be inversely proportional to the mobile hole concentration. However, we can state this relationship only qualitatively in the absence of data on the O content, since it was not measured. Clearly, more detailed studies in this direction are necessary to explain this relationship and its implications for high-temperature superconductivity.

Acknowledgments

Valuable help by D D Choughule, Department of Physics, University of Poona, during this work is gratefully acknowledged. One author, SKD, would like to thank CSIR, New Delhi, for a Senior Research Fellowship. Financial support by the Programme Management Board (PMB) of DST (Government of India) is also gratefully acknowledged

References

[1] Beno M A, Soderholm L, Capone D W II, Hinks D G, Jorgensen J D, Grace J D, Schuller I K, Segre C U and Zhang K 1987 *Appl. Phys. Lett.* **51** 57

[2] Tarascon J M, Barboux P, Miceli P F, Greene L H, Hull G W, Eibschutz M and Sunshine S A 1988 *Phys. Rev.* B **37** 7458

[3] Maeno Y, Tomita T, Kyogoku M, Awaji S, Aoki K, Hoshino K, Minami A and Fujita T 1987 *Nature* **328** 512

[4] Takayama-Muromachi E, Uchida Y and Kato K 1987 *Japan. J. Appl. Phys.* **26** L2087

[5] Obara H, Oyanagi H, Murata K, Yamasaki H, Ihara H, Tokumoto M, Nishihara Y and Kimura Y 1988 *Japan. J. Appl. Phys.* **27** L6803

[6] Xu Y, Suenaga M, Tafto J, Sabatini R L, Moodenbaugh A R and Zolliker P 1989 *Phys. Rev.* B **39** 6667

[7] Maeda H, Koizumi A, Bamba N, Takayama-Muromachi E, Izumi F, Asano H, Shimizu K, Moriwaki H, Maruyama H, Kuroda Y and Yamazaki H 1990 *Physica* C **157** 483

[8] Shaked H, Faber J Jr, Veal B W, Hitterman R L and Paulikas A P 1990 *Solid State Commun.* **75** 445

[9] Yang C Y, Heald S M, Tranquada J M, Xu Youwen, Wang Y L, Moodenbaugh A R, Welch D O and Suenaga M 1989 *Phys. Rev.* B **39** 6681

[10] Oyanagi H, Obara H, Yamaguchi H, Murata K, Ihara H, Matsushita T, Tokumoto M, Nishihara Y and Kimura Y 1989 *J. Phys. Soc. Japan* **58** 2140

[11] Koizumi A, Maeda H, Bamba N, Maruyama H, Takayama-Muromachi E, Shi J, Shimizu K, Mino M and Yamazaki H 1989 *Japan. J. Appl. Phys.* **28** L203

[12] Padalia B D, Gurman S J, Mehta P K and Om Prakash 1992 *J. Phys.: Condens. Matter* **4** 6865

[13] Deshpande S K, Chaudhari S M, Pimpale Ashok, Nigavekar A S, Ogale S B and Bhide V G 1991 *Pramana–J. Phys.* **37** 373

[14] Aldea N and Indrea E 1990 *Comput. Phys. Commun.* **60** 145

[15] Sayers D E and Bunker B A 1988 *X-ray Absorption: Principles, Applications, Techniques of EXAFS, SEXAFS and XANES* ed D C Koningsberger and R Prins (New York: Wiley) p 211

[16] Cook J W Jr and Sayers D E 1981 *J. Appl. Phys.* **52** 5024

[17] Stern E A 1988 *X-ray Absorption: Principles, Applications, Techniques of EXAFS, SEXAFS and XANES* ed D C Koningsberger and R Prins (New York: Wiley) p 3

[18] Cramer S P, Hodgson K O, Stiefel E I and Newton W E 1978 *J. Am. Chem. Soc.* **100** 2748

[19] Zhao Y, Liu H K, Yang G and Dou S X 1993 *J. Phys.: Condens. Matter* **5** 3623

[20] Tokura Y, Torrance J B, Huang T C and Nazzal A I 1988 *Phys. Rev.* B **38** 7156